Journal of Alloys and Compounds 867 (2021) 158986

Contents lists available at ScienceDirect

Journal of Alloys and Compounds

journal homepage: www.elsevier.com/locate/jalcom

Optical thermometry based on thermolabile intrinsic polarons in Tm^{3+} and Yb^{3+} co-doped congruent lithium niobate single crystal

Zhihua Liu[b], Siwei Long[a,*], Yunzhong Zhu[b], Wenjia Wang[a], Biao Wang[a,b,**]

[a] School of Physics, Sun Yat-sen University, Guangzhou 510275, China
[b] Sino French Institute of Nuclear Engineering and Technology, Sun Yat-sen University, Zhuhai 519082, China

ARTICLE INFO

Article history:
Received 11 October 2020
Received in revised form 5 January 2021
Accepted 28 January 2021
Available online 1 February 2021

Keywords:
Temperature sensing
Non-thermally coupled levels
Lithium niobate
Upconversion emission
Thermolabile polarons

ABSTRACT

By contrast with the conventional optical thermometry based on fluorescence intensity ratio (FIR) of thermally coupled levels (TCLs), we propose a novel thermometry strategy based on the diversity in thermal responses of non-TCLs of Tm^{3+} ($^3H_4 \rightarrow {}^3H_6/{}^1G_4 \rightarrow {}^3F_4$). Notably, the exacerbated response-contrast stems from the intrinsic structure variation induced by thermolabile polarons of and Nb_{Nb}^{4+} in congruent Tm^{3+},Yb^{3+}:$LiNbO_3$(LN) single crystal. The luminescence mechanism incorporated with energy transfer processes associated with polarons levels is revealed by investigating the abnormal temperature dependence of emission spectra under 980 nm excitation. The maximum absolute (S_A) and relative (S_R) sensitivities reach as high as 3.7% K^{-1} and 1.25% K^{-1} at 80 K, much higher than those of the TCLs strategy based on thermally coupled Stark sublevels of Tm^{3+} ($^3H_4|1 \rightarrow {}^3H_6/{}^3H_4|3 \rightarrow {}^3H_6$) in Tm^{3+},Yb^{3+}:LN. This study demonstrates an effective pathway for developing new FIR strategies with improved sensitivities *via* taking advantage of host structure variation.

1. Introduction

Temperature detection has always been a vital subject in industrial manufacture and scientific research. Conversional thermal detection strategies, such as thermistors and thermocouples, commonly require physical contact, which hampers the application in ultra-high temperature and strongly corrosive environment [1,2]. Alternatively, non-contact optical thermometer has attracted intense attention due to plenty of remarkable advantages such as high resolution, fast response and wide applicability in harsh-environments/dynamic-systems [3–5]. A variety of optical thermometers have been proposed based on temperature dependent optical parameters, including fluorescence intensity ratio (FIR) [6,7], fluorescence intensity (FI) [8], wavelength [9] and radiative lifetime [10]. Notably, FIR strategy possesses prominent accuracy and reliability *via* self-referencing, thus receiving the most attention and study [11,12]. In principle, FIR strategy refers to the ratio of integrated emission intensities of two associated levels. According to the energy gap between the two involved levels, the FIR strategy is divided into two categories, that is, thermally coupled energy levels (TCLs) and non-TCLs [13,14]. Excited population distribution between the adjacent TCLs strictly follows Boltzmann law, which forms a basis of temperature reading. Accordingly, the relative sensitivity S_R, which is important for evaluating temperature sensing performance, is proportional to the energy gap of the TCLs. Nevertheless, S_R of TCLs strategy is limited by the confined energy gap (200 $cm^{-1} \leq \Delta E \leq 2000\ cm^{-1}$) which is essential to avoid de-coupling of TCLs and deviation from Boltzmann distribution of excited population [1,15]. With higher S_R inaccessible in theory, the intrinsic drawback severely hiders further improvement of TCLs strategy. Different from the TCLs strategy, non-TCLs strategy developed based on new sensing mechanism offers the possibility of overcoming the intrinsic drawback to reach a higher S_R. Thus, great effort has been devoted to developing novel non-TCLs strategies. For example, the maximum absolute sensitivity of 0.94%K^{-1} at 298 K has been achieved based on FIR associated with excited non-TCLs $^5F_5$ and $^5F_4/{}^5S_2$ of Ho^{3+} in Yb^{3+}/Ho^{3+} co-doped Lu_3NbO_7 phosphors [16]. A non-TCLs strategy was proposed with high temperature sensitivity of 15–22%K^{-1} based on dual emitting centers Cr^{3+}/Ln^{3+} (Ln=Eu, Tb, Dy) coupled with suppressed detrimental energy transfer between each other. Moreover, transitions of Eu^{2+}:5d→4f and Eu^{3+}:$^5D_0 \rightarrow {}^7F_J$($J$ = 1, 2, 4) have been utilized for significantly improved S_R of 4%K^{-1} *via* partial reduction of Eu^{3+} into Eu^{2+} in YF_3 glass ceramic [17]. However, considering the maximum S_R of 0.94%K^{-1} in Yb^{3+}/Ho^{3+} co-doped Lu_3NbO_7 is

* Corresponding author.
** Corresponding author at: School of Physics, Sun Yat-sen University, Guangzhou 510275, China.
E-mail addresses: longsw3@mail.sysu.edu.cn (S. Long), wangbiao@mail.sysu.edu.cn (B. Wang).

https://doi.org/10.1016/j.jallcom.2021.158986
0925-8388/

relatively low, better sensing performance is expected in our work. In spite of excellent S_R more achievable in dual-emitting-center systems Cr^{3+}/Ln^{3+}, FIR originated from dual activators would be less favorable for the control of temperature sensing performance. The emissions originating from the high energy level of Eu^{2+}:5d in YF_3 are specially applied in thermometry at the blue light range. Besides, these three non-TCLs strategies employ only the characteristic features of emitting centers without taking advantage of the host structure variation. Here, a novel non-TCLs strategy developed *via* coupling temperature dependent energy transfer associated with host structure variation to luminescence route might provide a new way for high temperature sensitivity but are rarely explored. Based on 4*f*-4*f* transitions originating from one activator, the novel non-TCLs strategy might operate in red light and NIR range with better control of temperature sensing performance.

The versatile perovskite crystal lithium niobate (LN) exhibiting predominant properties of thermostability, low cut-off phonon energy, acid and alkali proof, has been demonstrated to be a promising host material for optical thermometer [18,19]. In congruent LN (Li/Nb = 0.946), plentiful anti-position Nb (Nb_{Li}^{4+}) and Li-vacancy (V_{Li}^{-}) stemming from crystal distortion due to the deviation in composition from the stoichiometry are distributed in crystal lattice [20]. Interestingly, Nb_{Li}^{4+} and normal Nb (Nb_{Nb}) would capture electrons from V_{Li}^{-}, forming Nb_{Li}^{3+} and Nb_{Nb}^{4+} polarons which are unstable at room temperature but gradually stabilize with decreasing temperature to around 120 K [21]. Moreover, the energy levels of Nb_{Li}^{3+} and Nb_{Nb}^{4+} polarons are located 1.2 and 1.6 eV below the bottom of conduction band (CBB), matching to the transition energy related to Yb^{3+}: $^2F_{5/2}\rightarrow{}^2F_{7/2}$ and Tm^{3+}: $^3H_4\rightarrow{}^3H_6$, respectively [22,23]. Therefore, it is expected that the temperature dependent $Nb_{Nb}^{4+}/Nb_{Li}^{3+}$ polarons may be utilized for manipulation of the luminescence intensity ratio *via* modifying upconversion (UC) luminescence mechanisms in Tm^{3+},Yb^{3+}:LN, which provides theoretical basis for a non-TCLs strategy with an improved S_R.

In this work, the structure of as grown Tm^{3+},Yb^{3+}:LN single crystal is studied based on temperature dependent infrared absorption spectra for the characterization of thermally unstable Nb_{Li}^{3+} and Nb_{Nb}^{4+} polarons. The UC spectroscopic properties of Tm^{3+},Yb^{3+}:LN are studied. The UC luminescence mechanism incorporated with energy levels of Nb_{Li}^{3+} and Nb_{Nb}^{4+} polarons is investigated for accounting for the abnormal 'U' shape variation of emission intensity with increasing temperature. A novel non-TCLs FIR strategy (Tm^{3+} 800/651 nm) based on the temperature dependent polarons is presented for improved temperature sensitivity, in comparison with conventional TCLs FIR strategy (Tm^{3+} 797/819 nm).

2. Experiment

Lithium carbonate (Li_2CO_3), niobium oxide (Nb_2O_5), thulium oxide (Tm_2O_3), and ytterbium oxide (Yb_2O_3) of analytical grade (99.99%) are used for the synthesis of $LiNbO_3$ single crystal. The Li/Nb ratio in congruent Li_2O–Nb_2O_5 mixture is 0.946, while the concentrations of rare earth ions Tm^{3+} and Yb^{3+} are 0.2 and 0.5 mol% respectively. After mixing thoroughly, the powder is calcined at 900 °C for 1.5 h to decompose Li_2CO_3 and then 1150 °C for 6 h to form LN polycrystals. The Tm^{3+},Yb^{3+}:LN crystal is grown along c-axis from the melt in a Pt crucible by Czochralski (CZ) method. Fixed rotation speed of 15 rpm and pulling rate of 1 mm/hour are adopted. Wafers oriented perpendicular to b-axis are cut from the as-grown LN single crystal and polished for optical tests.

The infrared absorption spectra are measured within the wavenumber range of 4500–600 cm^{-1} using a Fourier transformation infra-red spectrometer (PerkinElmer Spectrum100SystemB). The photoluminescence spectra are recorded by a Photoluminescence Spectrometer (OmniFluo990) equipped with a 980 nm semiconductor laser as excitation source. For the spectroscopic measurements at the temperature ranging from 80 to 260 K, a liquid-nitrogen cooled cryostat (OXFORD OptistatDN2) is used.

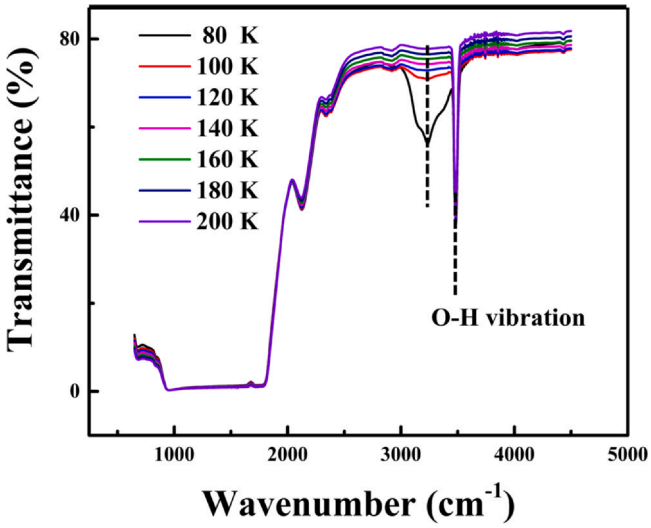

Fig. 1. The infrared absorption spectra recorded from 80 to 260 K.

3. Result and discussion

The intrinsic structure of congruent LN single crystal is characterized by infrared absorption spectra from 80 to 260 K, as shown in Fig. 1. There are two main absorption peaks centered at 3250 and 3500 cm^{-1}, which attribute to electron transition between levels of polarons Nb_{Li}^{3+} and Nb_{Nb}^{4+} and O–H bond vibration, respectively. The absorption peak related to O–H bond vibration at 3500 cm^{-1} varies little with temperature, implying the impact on UC intensity is temperature independent. By contrast, sudden increase in intensity of absorption peak at 3250 cm^{-1} emerges with temperature decreasing from 120 to 80 K, indicating that the threshold temperature for stabilization of $Nb_{Nb}^{4+}/Nb_{Li}^{3+}$ polarons in congruent Tm^{3+},Yb^{3+}:LN is approximately 120 K [24,25].

The UC emission spectrum, containing luminescence characteristics of Tm^{3+},Yb^{3+}:LN single crystal, is measured under 980 nm continuous wave pumping, as shown in Fig. 2. The three main emission peaks centered at 475 (blue), 651 (red) and 800 (NIR) nm

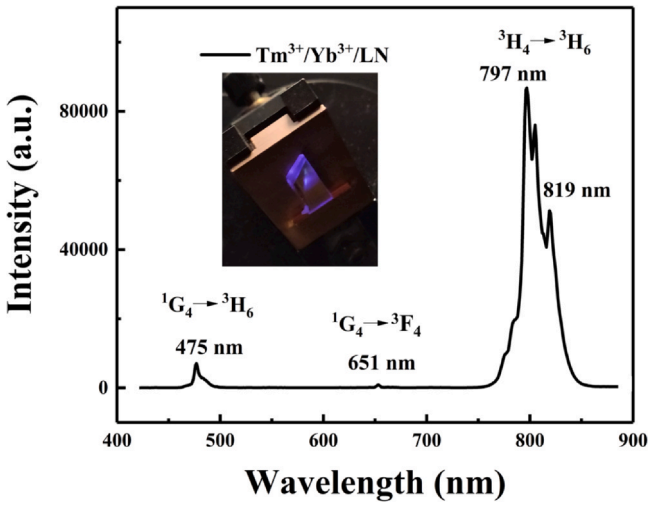

Fig. 2. The UC luminescence spectrum of Tm^{3+},Yb^{3+}:LN single crystal. The inset presents the photoluminescence photograph of Tm^{3+},Yb^{3+}:LN.

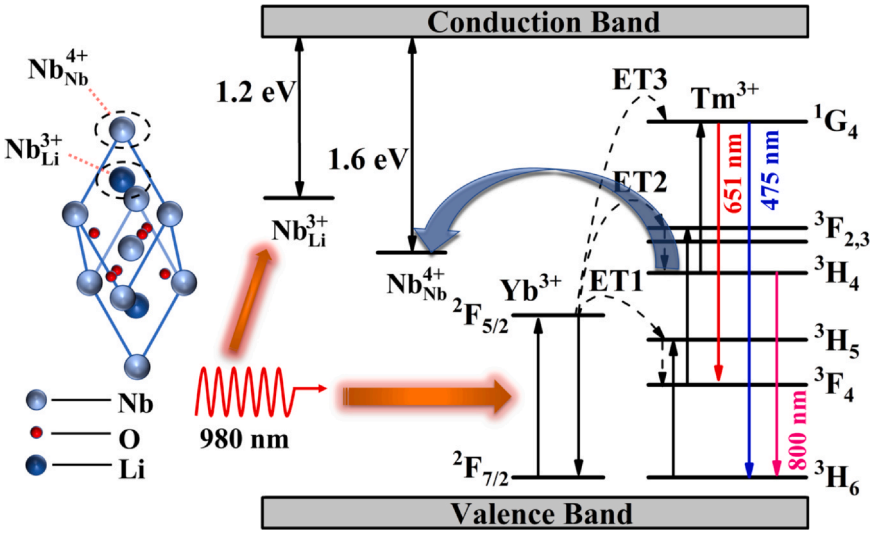

Fig. 3. The energy level diagram illustrating the luminescence mechanism in Tm^{3+},Yb^{3+}:LN under 980 nm excitation. (For interpretation of the references to colour in this figure legend, the reader is referred to the web version of this article.)

are attributed to the transitions of Tm^{3+}: $^1G_4 \rightarrow {}^3H_6$, $^1G_4 \rightarrow {}^3F_4$ and $^3H_4 \rightarrow {}^3H_6$, respectively. The photoluminescence photograph in the inset clearly demonstrates that bright blue light visible by the naked eye is obtained. The level diagram of Tm^{3+},Yb^{3+}:LN depicting the UC mechanism is illustrated in Fig. 3. Both the blue and red UC emissions involve a three-photon process [26–28], in which sensitizer Yb^{3+} continuously absorbs 980 nm pump light, excited from ground state to excited state (Yb^{3+}:$^2F_{7/2} \rightarrow {}^2F_{5/2}$), and then transfers the energy to luminescence center Tm^{3+} *via* ET1, 2 and 3 processes. To be specific, firstly, the ground state electron of Tm^{3+} is excited to $^3H_5$ level *via* ET1 process (Tm^{3+}:$^3H_6 \rightarrow {}^3H_5$), followed by non-radiative relaxation to $^3F_4$ level (Tm^{3+}:$^3H_5 \rightarrow {}^3F_4$). Then, electron at $^3F_4$ level continues accepting energy from Yb^{3+} *via* ET2 process and is promoted to $^3F_{2,3}$ level (Tm^{3+}:$^3F_4 \rightarrow {}^3F_{2,3}$), followed by non-radiative relaxation to $^3H_4$ level (Tm^{3+}:$^3F_{2,3} \rightarrow {}^3H_4$). After that, electron at $^3H_4$ level is excited to $^1G_4$ level *via* ET3 process (Tm^{3+}:$^3H_4 \rightarrow {}^1G_4$). Finally, efficient radiative transitions from $^1G_4$ to $^3H_6$ and $^3F_4$ levels occur, accompanied by strong blue (Tm^{3+}:$^1G_4 \rightarrow {}^3H_6$) and red emissions ($Tm^{3+}$:$^1G_4 \rightarrow {}^3F_4$).

It is expected that the density variation of $Nb^{4+}_{Nb}/Nb^{3+}_{Li}$ polarons with temperature may alter the temperature dependency of UC emission of Tm^{3+}, which could build a basis for non-TCLs FIR thermometry. Hence, the UC spectra are measured under excitation of 980 nm diode laser with a fixed pump power (800 mW) from 80 to 260 K, as presented in Fig. 4. Abnormal 'U' shape variation of luminescence intensity *versus* temperature is observed for the blue, red and NIR emission peaks. With peak positions invariant, the overall intensities of all the emission peaks decrease firstly from 80 to 120 K, and then turn to increase until 260 K, in contrast to a monotonous decrease driven by phonon-assisted non-radiative relaxation from the excited level in general cases. With a view to the coincidence between inflection temperature of UC intensity variation and threshold temperature for stabilization of $Nb^{4+}_{Nb}/Nb^{3+}_{Li}$ polarons, it is speculated that the abnormal intensity variation is closely linked to the LN structure variation. As depicted in Fig. 3, the energy gap between Nb^{3+}_{Li} level and the CBB of 1.2 eV matches well with the energy of 980 nm excitation beam, leaving a competition of accepting pump energy against the UC process relying on the

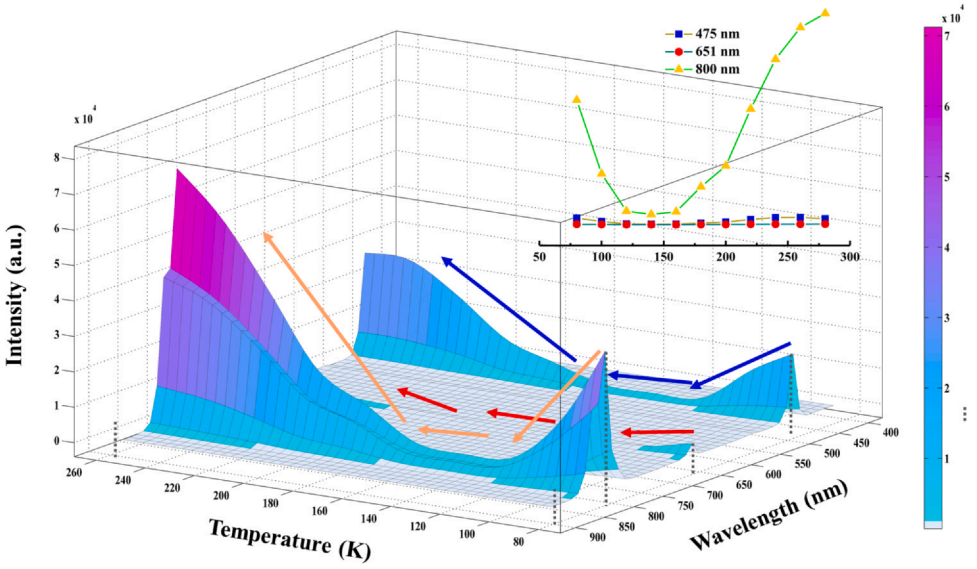

Fig. 4. The UC spectra of Tm^{3+},Yb^{3+}:LN at temperatures ranging from 80 to 260 K. The inset presents integral intensities of 475, 651 and 800 nm emission peaks. (For interpretation of the references to colour in this figure legend, the reader is referred to the web version of this article.)

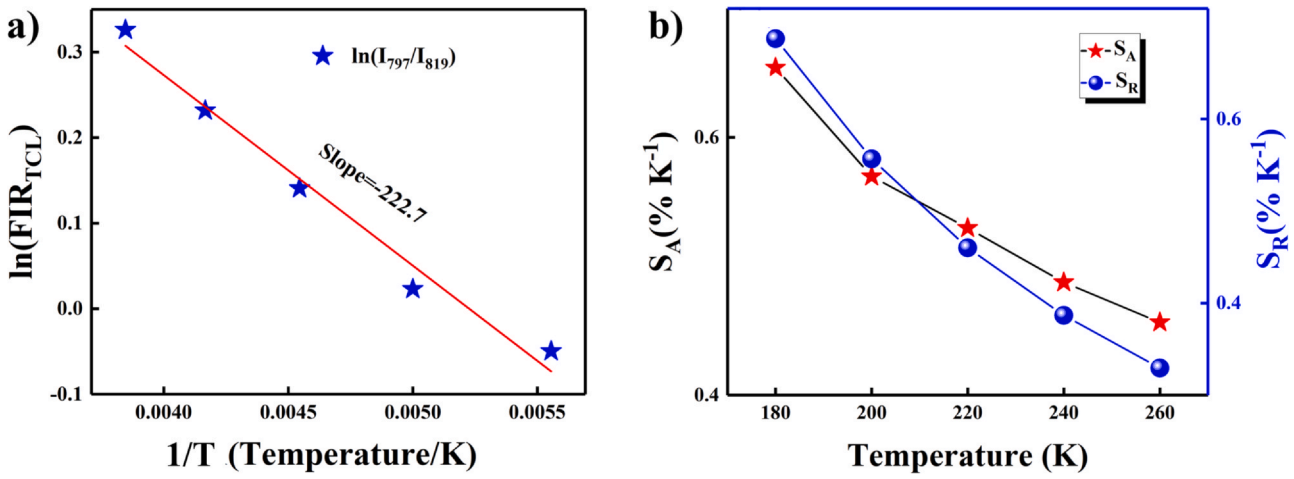

Fig. 5. (a) The ln(FIR) *versus* 1/*T* at the temperature range of 180–260 K, (b) S_A and S_R of the TCLs technique.

stabilized Nb_{Li}^{3+} polaron below 140 K. When the temperature is elevated above 140 K, the reduction of Nb_{Li}^{3+} polaron is to the benefit of the absorption of excitation light in Tm^{3+}, accompanied with an increase of UC intensity, which accounts for the abnormal 'U' shape intensity variation in Tm^{3+},Yb^{3+}:LN. Besides, as depicted in Fig. 3, the energy matching of 1.6 eV induces a probability increase of energy transfer between Tm^{3+}:$^3H_4 \rightarrow {}^3H_6$ and $Nb_{Nb}^{4+} \rightarrow$CBB, which is inimical to the 800 nm emission at temperatures below 140 K. At above 140 K, due to the reduction of Nb_{Nb}^{4+} polaron, a further intensity increase occurs for the 800 nm emission. As a result, the same 'U' shape variation *versus* temperature with significantly greater variation amplitude is observed for the 800 nm emission in comparison to the 475 and 651 nm emission. The discrepancy in thermal respond associated with LN structure variation offers a possibility for a novel non-TCLs strategy.

To assess the feasibility of non-TCLs optical thermometer, the performance of TCLs strategy in Tm^{3+},Yb^{3+}:LN is evaluated firstly as a comparison. The common strategy based on TCLs of Tm^{3+}:$^3F_{2,3}$ and $^3H_4$ is not available in Tm^{3+},Yb^{3+}:LN since the emission related to $^3F_{2,3}$ is too weak to be detected. Alternatively, the Stark sublevels of $^3H_4$ level are adopted for FIR noncontact thermometry. The FIR originating from TCLs, the population distribution of which obeys Boltzmann's law [29], could be expressed as:

$$FIR_{TCL} = \frac{I_{797}}{I_{819}} = B\exp\left(\frac{-\Delta E}{k_B T}\right) \quad (1)$$

where I_{797} and I_{819} are the integrated intensities corresponding to the $^3H_4|1 \rightarrow {}_3H_6$ and $^3H_4|3 \rightarrow {}^3H_6$ transitions, respectively. ΔE is the energy gap between TCLs. k_B is Boltzmann constant and T represents the absolute temperature. For a more intuitive understanding of the temperature dependence of FIR, Eq. (1) could be transformed into natural logarithm expression:

$$\ln(FIR_{TCL}) = \frac{-\Delta E}{k_B T} + \ln(B) \quad (2)$$

The dependence of ln(FIR) on 1/T at the temperature range of 180–260 K is shown in the Fig. 5(a). The experimental data shows linear variation behavior with a slope of −222.7 K^{-1}. The absolute sensitivity (S_A) and relative sensitivity (S_R), which are vital parameters for characterizing the temperature sensing performance, could be derived by the Eqs. (3) and (4) respectively as follows:

$$S_A = \frac{dFIR}{dT} = FIR\frac{\Delta E}{k_B T^2} \quad (3)$$

$$S_R = \frac{1}{FIR}\frac{dFIR}{dT} = \frac{\Delta E}{k_B T^2} \quad (4)$$

The maximum S_A and S_R are 0.65% and 0.69%K^{-1} at 180 K, as shown in the Fig. 5(b). As for the non-TCLs thermometry, a strategy based on FIR of I_{800} ($^3H_4 \rightarrow {}^3H_6$)/$I_{651}$ ($^1G_4 \rightarrow {}^3F_4$) is proposed. With similar thermal respond but smaller intensity as presented in the inset of Fig. 4, red emission I_{651} rather than blue emission I_{475} is preferred for higher temperature sensitivities. The experimental value of FIR I_{800}/I_{651} *versus* the reciprocal of temperature at temperatures below and above 160 K is linear fitted, as presented in Fig. 6(a) and (b), with a slope of − 64,795.3 and 23,684.1 K, respectively. To demonstrate the repeatability of this measurement, Fig. 6(c) presents the temperature-induced switching for R(I_{800}/I_{651}) (from 80 to 140 K), which indicates the repeatable and reversible of our measurement. The corresponding results of S_A and S_R at temperatures below and above 160 K are presented in Fig. 5(c) and (d) with maximum S_A of 3.7% K^{-1} and maximum S_R of 1.25% K^{-1} at 80 K. The temperature uncertainties δT are determined based on Eq. (5) [30].

$$\delta T = \frac{1}{S_R} \times \frac{\delta FIR}{FIR}. \quad (5)$$

The deviation $\delta FIR/FIR$ of I_{800}/I_{651} during heating and cooling processes is determined to be smaller than 0.625%. The minimum temperature uncertainty δT is calculated to be 0.50 K at 80 K.

A comparison of the thermometry performance among the FIR strategies, including the proposed non-TCLs (Tm^{3+}: I_{800}/I_{651}) strategy, TCLs strategy (Tm^{3+}: I_{797}/I_{819}) in Tm^{3+},Yb^{3+}:LN and other FIR strategies based on Ln^{3+} doped materials reported recently in the literature, is presented in Table 1. In Tm^{3+},Yb^{3+}:LN single crystal, the non-TCLs strategy demonstrates a better performance than the TCLs one within the measurement temperature range. We note that the temperature sensing performance of the proposed non-TCLs strategy (Tm^{3+}:I_{800}/I_{651}) still needs further improvement to compete with the state-of-the-art ones. However, with the satisfying maximum S_R of 1.25%K^{-1} achieved, the proposed non-TCLs strategy is demonstrated to be superior to most of the reported FIR thermometer in the literature. The above results indicate that Tm^{3+},Yb^{3+}:LN single crystal is a promising material for low temperature optical thermometer. Moreover, this strategy by virtue of modification of UC process *via* variation of host structure offer a new way to explore new materials for optical thermometry with high performance.

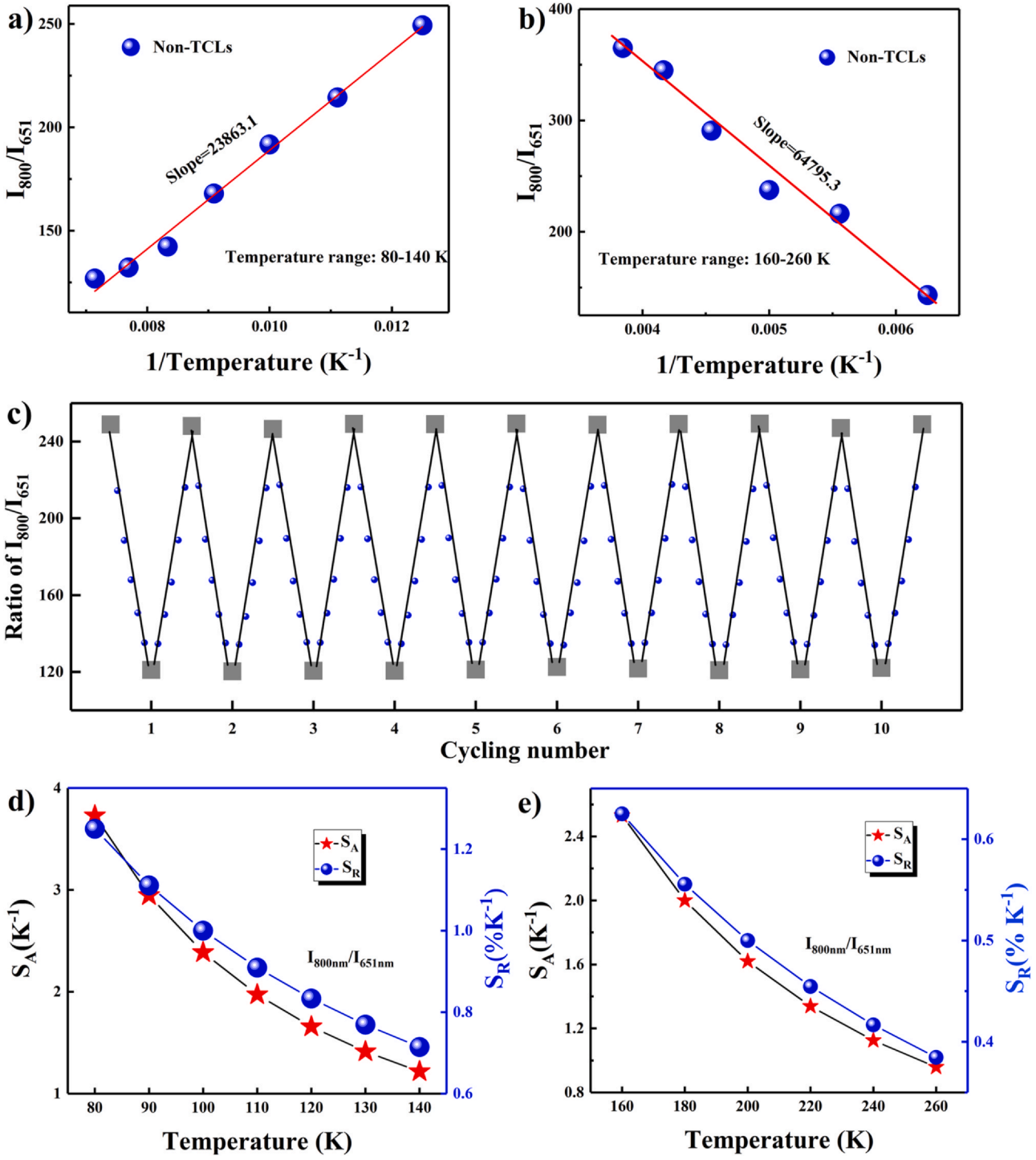

Fig. 6. The fluorescence intensity ratio of I_{800}/I_{651} *versus* $1/T$ at the temperature range of (a) 80–140 K, (b) 160–260 K. (c) The temperature-induced switching of R(I_{800}/I_{651}) (from 80 to 140 K), The absolute and relative sensitivities of I_{800}/I_{651} at the temperature range (d) 80–140 K, (e) 160–260 K.

4. Conclusion

In summary, we present a novel non-TCLs strategy for optical thermometry in Tm^{3+},Yb^{3+}:LN single crystal with improved temperature sensitivity based on temperature dependent $Nb_{Nb}^{4+}/Nb_{Li}^{3+}$ polarons. Firstly, the structure property is characterized by temperature dependent infrared absorption spectra. The thermal instability of $Nb_{Nb}^{4+}/Nb_{Li}^{3+}$ polarons at temperatures above 120 K is demonstrated. Then, the temperature dependent emission spectra are studied to reveal the UC luminescence mechanism. Notably, the energy levels of $Nb_{Nb}^{4+}/Nb_{Li}^{3+}$ polarons incorporated in the UC process are speculated to account for the abnormal 'U' shape variation of UC intensity and especially greater variation amplitude at 800 nm with increasing temperature. In comparison with the TCLs strategy (Tm^{3+} I_{797}/I_{819} nm), the non-TCLs strategy (Tm^{3+}: I_{800}/I_{651}) presents improved thermometry performance with maximum S_A of 3.7% K^{-1} and maximum S_R of 1.25% K^{-1} at 80 K. This result indicates that Tm^{3+},Yb^{3+}:LN single crystal is a promising material for low

Table 1
Comparison of various Ln^{3+}-doped systems used in non-TCLs and TCLs FIR luminescence thermometry.

Temperature sensing materials	Luminescence center	Type	Maximum S_R (%K^{-1})	Range ΔT (K)	Reference
Tm^{3+},Yb^{3+}:LN	Tm^{3+} (I_{800}/I_{651})	non-TCLs	1.25	80–160	this work
Tm^{3+},Yb^{3+}:LN	Tm^{3+} (I_{797}/I_{819})	TCLs	0.69	180–260	this work
Er^{3+},Yb^{3+}:$NaYF_4$	Er^{3+} (I_{525}/I_{545})	TCLs	1.24	298–693	[31]
Er^{3+},Yb^{3+},Fe^{3+}:$NaBiF_4$	Er^{3+} (I_{525}/I_{546})	TCLs	0.53	303–543	[32]
Er^{3+},Tm^{3+},Yb^{3+}:La_2ZnTiO_6	Er^{3+} (I_{532}/I_{546})	TCLs	0.54	298–574	[33]
Tm^{3+},Yb^{3+}: Sr_2YF_7	Tm^{3+} (I_{700}/I_{650})	TCLs	1.16	303–663	[34]
Ho^{3+}:Lu_3NbO_7	Ho^{3+} (I_{668}/I_{759})	non-TCLs	0.94	298–523	[16]
Er^{3+}:Y_2WO_6	Er^{3+} (I_{662}/I_{540})	non-TCLs	1.17	303–563	[35]
Ho^{3+}:$Ba_3Y_4O_9$	Ho^{3+}(I_{550}/I_{668})	non-TCLs	0.36	294–573	[36]
Eu^{2+},Eu^{3+}:YF_3	Eu (I_{425}/I_{611})	non-TCLs	4.12	300–563	[17]

temperature optical thermometer. Moreover, the proposed non-TCLs strategy demonstrates a new way to explore new temperature sensing materials *via* variation of host structure.

CRediT authorship contribution statement

Zhihua Liu: Conceptualization, Writing - original draft preparation, Methodology. **Siwei Long:** Writing - review & editing, Methodology, Data analysis. **Yunzhong Zhu:** Experiment. Wenjia Wang: Experiment. **Biao Wang:** Writing - review & editing, Supervision.

Declaration of Competing Interest

The authors declare that they have no known competing financial interests or personal relationships that could have appeared to influence the work reported in this paper.

Acknowledgment

This work was supported by the National Natural Science Foundation of China (NSFC) (11832019, 51802358), National Natural Science Foundation of Guangdong Province (2018A030313321, 2017A030310426), Fundamental Research Funds for the Central Universities (19lgpy273), Science and Technology Program of Guangzhou (201904010246) and National Doctoral Program Fund (20130171130003).

References

[1] X. Wang, Q. Liu, Y. Bu, C.S. Liu, T. Liu, X. Yan, Optical temperature sensing of rare-earth ion doped phosphors, RSC Adv. 5 (2015) 86219–86236.
[2] C. Jin, J. Zhang, Upconversion luminescence of $Ca_2Gd_8(SiO_4)_6O_2$:Yb^{3+}-Tm^{3+}-Tb^{3+}/Eu^{3+} phosphors for optical temperature sensing, Opt. Laser Technol. 115 (2019) 487–492.
[3] G.Z. Sui, X.P. Li, L.H. Cheng, J.S. Zhang, J.S. Sun, H.Y. Zhong, Y. Tian, S.B. Fu, B.J. Chen, Laser cooling with optical temperature sensing in Er^{3+}-doped tellurite-germanate glasses, Appl. Phys. B Lasers Opt. 110 (2013) 471–476.
[4] P. Du, L.H. Luo, W.P. Li, Q.Y. Yue, H.B. Chen, Optical temperature sensor based on upconversion emission in Er-doped ferroelectric $0.5Ba(Zr_{0.2}Ti_{0.8})O_3$-$0.5(Ba_{0.7}Ca_{0.3})TiO_3$ ceramic, Appl. Phys. Lett. 104 (2014) 152902.
[5] K.Z. Zheng, W.Y. Song, G.H. He, Z. Yuan, W.P. Qin, Five-photon UV upconversion emissions of Er^{3+} for temperature sensing, Opt. Express 23 (2015) 7653–7658.
[6] M. Runowski, A. Bartkowiak, M. Majewska, I.R. Martín, S. Lis, Upconverting lanthanide doped fluoride $NaLuF_4$:Yb^{3+}-Er^{3+}-Ho^{3+}-optical sensor for multi-range Fluorescence Intensity Ratio (FIR) thermometry in visible and NIR regions, J. Lumin. 201 (2018) 104–109.
[7] M.A. Hernández-Rodríguez, A.D. Lozano-Gorrín, I.R. Martín, U.R. Rodríguez-Mendoza, V. Lavín, Comparison of the sensitivity as optical temperature sensor of nano-perovskite doped with Nd^{3+} ions in the first and second biological windows, Sens. Actuators B 255 (2018) 970–976.
[8] A.H. Khalid, K. Kontis, Thermographic phosphors for high temperature measurements: principles, current state of the art and recent applications, Sensors 8 (2008) 5673–5744.
[9] K. Binnemans, Lanthanide-based luminescent hybrid materials, Chem. Rev. 109 (2009) 4283–4374.
[10] B.R. Rdeey, I. Kamma, P. Kommidi, Optical sensing techniques for temperature measurement, Appl. Opt. 52 (2013) B33eB39.
[11] Y. Liu, G. Bai, E. Pan, Y. Hua, L. Chen, S. Xu, Upconversion fluorescence property of Er^{3+}/Yb^{3+} codoped lanthanum titanate microcrystals for optical thermometry, J. Alloy. Compd. 822 (2020) 153449.
[12] C.D.S. Brites, P.P. Lima, N.J.O. Silva, A. Millán, V.S. Amaral, F. Palacio, L.D. Carlos, Thermometry at the nanoscale, Nanoscale 4 (2012) 4799.
[13] Y. Gao, F. Huang, H. Lin, J. Zhou, J. Xu, Y. Wang, A novel optical thermometry strategy based on diverse thermal response from two intervalence charge transfer states, Adv. Funct. Mater. 26 (2016) 3139–3145.
[14] M. Runowski, N. Stopikowska, D. Szeremeta, S. Goderski, M. Skwierczyńska, S. Lis, Upconverting lanthanide fluoride core@shell nanorods for luminescent thermometry in the first and second biological windows: β-$NaYF_4$:Yb^{3+}–Er^{3+}@SiO_2 temperature sensor, ACS Appl. Mater. Interfaces 11 (2019) 13389–13396.
[15] M. Runowski, A. Shyichuk, A. Tymiński, T. Grzyb, V. Lavín, S. Lis, Multifunctional optical sensors for nanomanometry and nanothermometry: high-pressure and high-temperature upconversion luminescence of lanthanide-doped phosphates-$LaPO_4$/YPO_4:Yb^{3+}–Tm^{3+}, ACS Appl. Mater. Interfaces 10 (2018) 17269–17279.
[16] J. Liao, L. Kong, M. Wang, Y. Sun, G. Gong, Tunable upconversion luminescence and optical temperature sensing based on non-thermal coupled levels of Lu_3NbO_7:Yb^{3+}/Ho^{3+} phosphors, Opt. Mater. 98 (2019) 109452.
[17] D. Chen, M. Xu, S. Liu, X. Li, Eu^{2+}/Eu^{3+} dual-emitting glass ceramic for self-calibrated opticalthermometry, Sens. Actuators B Chem. 246 (2017) 756–760.
[18] L. Xing, Y. Xu, R. Wang, W. Xu, Influence of temperature on upconversion multicolor luminescence in Ho^{3+}/Yb^{3+}/Tm^{3+}-doped $LiNbO_3$ single crystal, Opt. Lett. 38 (2013) 2535–2537.
[19] L. Arizmendi, Review article: photonic applications of lithium niobate crystals, Phys. Stat. Sol. 201 (2004) 253–283.
[20] Y.Z. Zhu, S.P. Lin, Y. Zheng, D.C. Ma, B. Wang, Improvement of pyroelectric figures of merit in zirconia-doped congruent lithium niobate single crystals, J. Mater. Sci. 51 (2016) 3155–3161.
[21] A. Harhira, L. Guilbert, P. Bourson, H. Rinnert, Polaron luminescence in iron-doped lithium niobate, Appl. Phys. B 92 (2008) 555–561.
[22] O.F. Schirmer, D. Vonder Linden, Two-photon- and x-ray-induced Nb^{4+} and O^- small polarons in $LiNbO_3$, Appl. Phys. Lett. 33 (1978) 35–38.
[23] Y. Qu, R. Wang, Z. Qiu, Y. Tao, J. Zhou, White-light upconversion emissions and color tunability of $12CaO{\cdot}7Al_2O_3$:Ho^{3+}/Yb^{3+}/Tm^{3+}, Opt. Mater. Express 5 (2015) 1881–1889.
[24] G.K. Kitaeva, K.A. Kuznetsov, A.N. Penin, A.V. Shepelev, Influence of small polarons on the optical properties of Mg:$LiNbO_3$ crystals, Phys. Rev. B 65 (2002) 054304.
[25] A. Harhira, L. Guilbert, P. Bourson, H. Rinnert, Polaron luminescence in iron-doped lithium niobate, Appl. Phys. B 92 (2008) 555–561.
[26] Y. Li, Y. Li, R. Wang, W. Zheng, Effect of silica surface coating on the luminescence lifetime and upconversion temperature sensing properties of semiconductor zinc oxide doped with gallium(III) and sensitized with rare earth ions Yb(III) and Tm(III), Microchim. Acta 185 (2018) 197–205.
[27] F. Wang, R. Deng, J. Wang, Q. Wang, Y. Han, H. Zhu, X. Chen, X. Liu, Tuning upconversion through energy migration in core–shell nanoparticles, Nat. Mater. 10 (2011) 968–973.
[28] L. Tong, X. Li, R. Hua, L. Cheng, J. Sun, J. Zhang, S. Xu, H. Zheng, Y. Zhang, B. Chen, Optical temperature sensing properties of Yb^{3+}/Tm^{3+} co-doped $NaLuF_4$ crystals, Curr. Appl. Phys. 17 (2017) 999–1004.
[29] K. Li, D. Zhu, H. Lian, Up-conversion luminescence and optical temperature sensing properties in novel $KBaY(MoO_4)_3$:Yb^{3+},Er^{3+} materials for temperature Sensors, J. Alloy. Compd. 816 (2020) 152554.
[30] S. Balabhadra, M.L. Debasu, C.D.S. Brites, R.A.S. Ferreira, L.D. Carlos, Upconverting nanoparticles working as primary thermometers in different media, J. Phys. Chem. C 121 (2017) 13962–13968.
[31] S. Jiang, P. Zeng, L. Liao, S. Tian, H. Guo, Y. Chen, C. Duan, M. Yin, Optical thermometry based on upconverted luminescence in transparent glass ceramics containing $NaYF_4$:Yb^{3+}/Er^{3+} nanocrystals, J. Alloy. Compd. 617 (2014) 538–541.
[32] P. Du, Q. Zhang, X. Wang, L. Luo, W. Li, Upconversion luminescence, temperature sensing and internal heating behaviors of Er^{3+}/Yb^{3+}/Fe^{3+}-tridoped $NaBiF_4$ nanoparticles, J. Alloy. Compd. 805 (2019) 171–179.

[33] Y. Wu, F. Lai, B. Liu, Z. Li, T. Liang, Y. Qiang, J. Huang, X. Ye, W. You, Energy transfer and cross-relaxation induced multicolor upconversion emissions in $Er^{3+}/Tm^{3+}/Yb^{3+}$ doped double perovskite La_2ZnTiO_6 phosphors, J. Rare Earths 38 (2020) 130–138.

[34] W. Chen, F. Hu, R. Wei, Q. Zeng, L. Chen, H. Guo, Optical thermometry based on up-conversion luminescence of Tm^{3+} doped transparent Sr_2YF_7 glass ceramics, J. Lumin. 192 (2017) 303–309.

[35] J. Zhang, B.W. Ji, G.B. Chen, Z.H. Hua, Upconversion luminescence and discussion of sensitivity improvement for optical temperature sensing application, Inorg. Chem. 57 (2018) 5038–5047.

[36] S.F. Liu, H. Ming, J. Cui, S.B. Liu, W.X. You, X.Y. Ye, Y.M. Yang, H.P. Nie, R.X. Wang, High sensitive $Ln^{3+}/Tm^{3+}/Yb^{3+}(Ln^{3+} = Ho^{3+}, Er^{3+})$ tri-doped $Ba3Y_4O_9$ upconverting optical thermometric materials based on diverse thermal response from non-thermally coupled energy levels, Ceram. Int. 45 (2019) 1–10.